

The terminal bulk Lorentz factor of relativistic electron-positron jets.

N. Renaud and G. Henri

Laboratoire d'Astrophysique, Observatoire de Grenoble, BP 53X F-38041 Grenoble Cedex France

Accepted —. Received —

ABSTRACT

We present numerical simulation of bulk Lorentz factor of relativistic electron-positron jet driven by Compton rocket effect from accretion disc radiation. The plasma is assumed to have a power-law distribution $n_e(\gamma) \propto \gamma^{-s}$ with $1 < \gamma < \gamma_{max}$ and is continuously reheated to compensate for radiation losses. We include full Klein-Nishina (hereafter KN) cross section, and study the role of energy upper cut-off γ_{max} , spectral index s , and source compactness. We determine terminal bulk Lorentz factor in the case of supermassive black holes relevant to AGN and stellar black holes relevant to galactic microquasars. In the latter case, Klein-Nishina cross section effect are more important, and induce terminal bulk Lorentz factor smaller than in the former case. Our result are in good agreement with bulk Lorentz factors observed in galactic sources (GRS1915+105, GROJ1655-40) and extragalactic ones. Differences in scattered radiation and acceleration mechanism efficiency in AGN environment can be responsible for the variety of relativistic motion in those objects. We also take into account the influence of the size of the accretion disc; if the external radius is small enough, the bulk Lorentz factor can be as high as 60.

Key words: galaxies: active - galaxies: jets - radiation mechanism: miscellaneous - stars: individual: GRS1915+105, GROJ1655-40

1 INTRODUCTION

Superluminal motion observed in Active Galactic Nuclei (AGN), especially in the blazars class, seems to be closely linked with high-energy emission. Such motion was recently observed in the Galaxy (Mirabel & Rodriguez 1994, Hjellming & Rupen 1995, Tingay et al. 1995) in the so-called microquasars. Nevertheless differences are noticeable in those two cases. The latter systems were observed with small value of bulk Lorentz factor (around 2.5), while in the former ones values of about 10-20 are frequent. It is well known that the radiation pressure acting on electron-positron plasma in the vicinity of a near Eddington accreting object is very efficient to accelerate the plasma outwards, since the gravitational force is around 1000 times weaker than for an electron-proton plasma. However, Phinney (1987) has shown that for a realistic accretion disc emission, only moderate values of bulk Lorentz factors can be reached. Li & Liang (1996), have recently proposed that this mechanism could explain the relatively small $\gamma_b \sim 2.5$ observed in galactic objects. They considered plasma composed with both e^+e^- and e^-p and obtained the equation of motion using the Thomson cross section and including gravitation force. To explain higher values of γ_b , O'Dell (1981) proposed the so-called 'Compton rocket' effect, *i.e.* anisotropic Inverse Compton effect on a highly relativistic plasma. It was then argued (Phinney

1982) that because Compton cooling is always much more rapid than bulk acceleration, only small value of $\gamma_{b\infty}$ could be reached by this mechanism. However, taking into account that in the frame of the 'two-flow' model (Sol, Pelletier & Asséo 1989), a pair plasma could be reheated by the turbulence triggered by a surrounding jet (Henri & Pelletier 1991), Marcowith, Henri & Pelletier (1995) showed that the Compton rocket becomes much more efficient and accelerates pair plasma to Lorentz factor $\gamma_b \sim 10$. In another work Sikora et al. (1996) studied the radiation drag in AGN jets. They included relativistic electron-positron plasma accelerated *in situ* and relativistic protons which contribute to the inertia of the flow. They considered radiation emitted from an accretion disc, partially reprocessed by the outer part of the disc or by spherically distributed matter at a given distance from the central object. All Compton interactions were computed using Thomson cross section. They showed that in most cases jets should undergo radiation drag, and that the efficiency of this mechanism becomes important for purely pair plasma dominating the jet luminosity. The aim of this paper is to study how Compton rocket effect can accelerate a pure pair plasma in the vicinity of accretion disc, taking into account the full KN cross section. Following Marcowith et al. (1995), we consider a blob of e^+e^- pair plasma with an isotropic energy distribution in the comoving frame $n'_e(\gamma') \propto \gamma'^{-s}$, where s is the spectral index. We

assume that the acceleration process is efficient enough in the jet to get a stationary energy distribution. We assume that the dynamics of the pair plasma is decoupled from the electron proton component and we do not include gravitation force. The radiation field is coming from an accretion disc. We include KN corrections in the description of the Inverse Compton interactions. We study the influence of both compactness of the radiation source, spectral index and upper cut-off γ_{max} , and make then comparisons between AGN and galactic microquasars. We also consider the influence of scattered radiation by a Broad Line Region (BLR) and dusty torus around the central black hole. Finally we discuss the influence of accretion disc's size that could be relevant to the high value of bulk Lorentz factors.

2 COMPTON ROCKET EFFECT WITH KLEIN-NISHINA CORRECTIONS

2.1 Notations

All energies are measured in unit $m_e c^2$. We refer all quantities expressed in the blob rest frame by a prime $'$, all quantities in the particle rest frame by a star * and quantities in the disc frame are not labelled. Photon energies will be labelled by ε , and the unit direction vector by \mathbf{k} . We use the KN differential cross section (Rybicki & Lightman 1979) given by:

$$\frac{d\sigma}{d\varepsilon_1^* d\Omega_1^*} = \frac{3\sigma_T}{16} \left(\frac{\varepsilon_1^*}{\varepsilon^*} \right)^2 \left(\frac{\varepsilon_1^*}{\varepsilon^*} + \frac{\varepsilon^*}{\varepsilon_1^*} - \sin^2 \phi^* \right) \delta \left(\varepsilon_1^* - \frac{\varepsilon^*}{1 + \varepsilon^*(1 - \cos \phi^*)} \right).$$

$\sigma_T = \frac{8\pi}{3} r_e^2$ is the Thomson cross-section where $r_e = \frac{e^2}{4\pi\varepsilon_0 m_e c^2}$ is the electron classical radius. This expression applies to the scattering of a photon with energy ε^* and direction \mathbf{k}^* in a photon with energy ε_1^* and direction \mathbf{k}_1^* , and $\cos \phi^* = \mathbf{k}^* \cdot \mathbf{k}_1^*$.

2.2 The general picture

Figure 1 shows the general configuration of the model.

The pair plasma is assumed to be described in the bulk rest frame by an energy distribution $n'_e(z, \gamma') \propto \gamma'^{-s}$ for $\gamma_{min} < \gamma' < \gamma_{max}$, with s , γ_{min} and γ_{max} independent of z (see paragraph 3.2.1 for a further discussion of this assumption). The radiation force is due to soft photons coming from a standard accretion disc (Shakura & Sunyaev 1973) around a Schwarzschild black hole. The inner radius of the accretion disc is $r_i = 3r_g$ (where r_g is the Schwarzschild radius of the black hole). The outer radius r_e is a free parameter. We use the black-body approximation for the disc emission so that the specific intensity at a radius r is:

$$I_\nu(r) = B_\nu(T_{eff}(r)), \quad (1)$$

where B_ν is the Planck function and the effective temperature T_{eff} is given by:

$$T_{eff}(r) = \left(\frac{3GM\dot{M}}{8\pi\sigma r^3} \right)^{1/4} [1 - b(r_i/r)^{1/2}]^{1/4}. \quad (2)$$

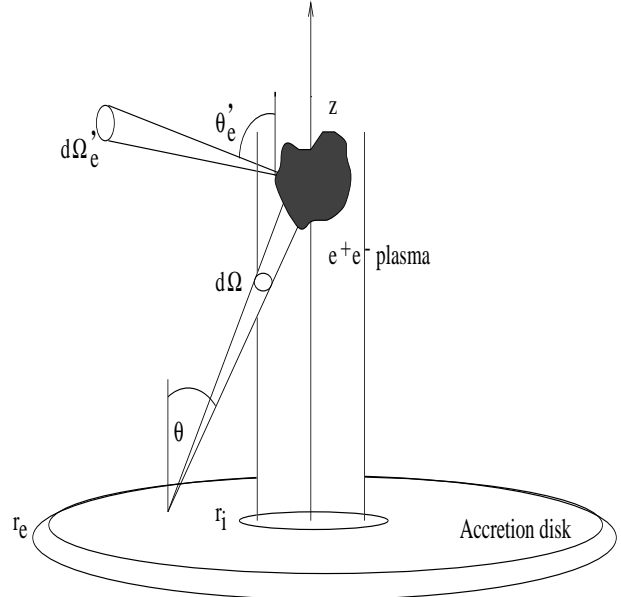


Figure 1. The general configuration of the model. Quantities in the blob rest frame are denoted by a prime.

\dot{M} is the accretion rate, M the mass of the central black hole and b is a parameter describing the inner torque on the disc ($0 \leq b \leq 1$). In section 4, we also consider the case of a two-temperatures disc model (Shapiro, Lightman & Eardley 1976). This model applies to the hot inner part of the disc ($r < a$ few r_g). The specific intensity is then (Sunyaev & Titarchuk 1980):

$$I_\nu(r) \propto \frac{\exp(-x)}{x} \left(1 + x + \frac{1}{2}x^2 + \frac{1}{6}x^3 + \frac{1}{24}x^4 \right) \text{ for } x > 1 \\ I_\nu(r) \propto x^4 \text{ for } x < 1, \quad (3)$$

where $x = h\nu/kT_e$ and T_e is the electronic temperature given by:

$$T_e(r) = 7.10^8 \text{ K} \left(\frac{M}{3M_\odot} \frac{10^{17} \text{ g.s}^{-1}}{\dot{M}} \right)^{1/6} [1 - (r_i/r)^{1/2}]^{-1/6} \\ \times (2r/r_g)^{1/4}. \quad (4)$$

In AGN, BLR surrounding the central black hole reprocesses a fraction of about 10 per cent of the disc radiation. In paragraph 3.2.5, following Sikora et al. (1996), we chose two extreme cases to describe this emission. The first case is case 'a' in Sikora et al. (1996) where a fraction χ of the total disc luminosity L_d is intercepted by the outer part of the disc and reprocessed in Ly α lines with a specific intensity given by:

$$I_\nu(r) = \frac{\chi L_d r^{-\alpha}}{4\pi^2 \int_{r_1}^{r_2} r^{1-\alpha} dr} g(\nu - \nu_{Ly\alpha}), \quad (5)$$

The radiation is re-emitted by a ring for $r_1 < r < r_2$. g is a rectangular profile with a Doppler width of $v/c \sim 2.24 \cdot 10^{-2}$. In the second case spherically distributed matter at a distance r_0 from the central engine reemits a fraction χ of the total disc luminosity. The emissivity of this radiation source

at a distance z on the jet axis is:

$$I_\nu(z, \theta) = \frac{\chi L_d}{4\pi r_0^2 \sqrt{1 + \left(\frac{z}{r_0}\right)^2 (\cos^2 \theta - 1)}} g(\nu - \nu_{\text{Ly}\alpha}), \quad (6)$$

For $z \leq r_0$, $-1 \leq \cos\theta \leq z/\sqrt{z^2 + r_0^2}$ and for $z > r_0$, $\sqrt{z^2 - r_0^2}/z \leq \cos\theta \leq 1$.

We also study the influence of possible scattered radiation from hot dust which may be responsible for near infrared emission in AGN. The emissivity of such a source modeled by a ring located between r_3 and r_4 can be expressed as follows :

$$I_\nu(r) = \frac{\chi' L_d}{4\pi \sigma \int_{r_3}^{r_4} T^4(r) r dr} B_\nu((T(r)), \quad (7)$$

T is the dust temperature, σ is the Stefan-Boltzmann constant, and χ' is the fraction of the disc luminosity that is reprocessed.

2.3 Computation of the radiative force

Let $\frac{dp'}{dt'}$ be the rates of momentum change for one electron due to Inverse Compton process and $\beta' c = \sqrt{1 - 1/\gamma'^2} c$ its velocity. The force exerted upon the pair plasma is then in the blob rest frame:

$$F'^z = \int d\Omega'_e d\gamma' n'_e(\gamma', \Omega'_e) \frac{dp'}{dt'} \cdot \mathbf{u}_z, \quad (8)$$

where \mathbf{u}_z defines the jet axis direction. This force is accompanied of course by an energy loss that tends to cool the plasma. However, as mentioned above, we assume that there exists a continuous acceleration mechanism that compensate for these losses, so that the particle distribution remains constant. We assume that this acceleration acts isotropically in the plasma frame, and so it does not contribute to the expression given in equation (8). We also neglect gravitation force, since for near-Eddington objects and cold pairs we have $\frac{F_{rad}}{F_{grav}} \sim \frac{m_p}{m_e} \sim 10^3$.

To calculate more easily F'^z , one can use two different approximations: for low energy particles, the KN cross-section tends to the Thomson limit and we can apply the result of Phinney (1982) for an isotropic pair plasma:

$$F'^z = \frac{\sigma_T}{c} 4\pi H' \int (1 + \frac{2}{3} \gamma'^2 \beta'^2) n'_e(\gamma') d\gamma', \quad (9)$$

where H' is the second Eddington parameter of the radiation field (Marcowith et al. 1995, see also Appendix A) defined in the blob rest frame. It is linked to the Eddington parameters defined in observer's rest frame by:

$$H' = \gamma_b^2 [(1 + \beta_b^2) H - \beta_b (J + K)], \quad (10)$$

where $\beta_b c$ is the bulk velocity and γ_b is the corresponding Lorentz factor. For high energy particles, KN corrections become important but we can assume the head-on approximation (Blumenthal & Gould 1970) to be valid. In this approximation, the velocity of all photons in the particle frame is assumed to be anti-parallel to the particle velocity in the observer frame. So the momentum loss rate is necessarily in

the direction of the particle motion. Let x denote this direction, the electron energy and momentum loss rate in its rest frame are in unit $m_e c^2$ (* refers to this frame):

$$\frac{dp_x^*}{dt^*} = - \int dn^* \frac{d\sigma}{d\varepsilon_1^* d\Omega_1^*} (\varepsilon^* - \varepsilon_1^* \cos \phi^*) d\varepsilon_1^* d\Omega_1^*, \quad (11)$$

and

$$\frac{dE^*}{dt^*} = -c \int dn^* \frac{d\sigma}{d\varepsilon_1^* d\Omega_1^*} (\varepsilon_1^* - \varepsilon^*) d\varepsilon_1^* d\Omega_1^*. \quad (12)$$

dn^* is the differential photon density in the electron rest frame. The momentum change rate in the blob rest frame is then given by:

$$\frac{dp'_x}{dt'} = \frac{dp_x^*}{dt^*} + \frac{\beta'}{c} \frac{dE^*}{dt^*}. \quad (13)$$

Note that using the KN cross-section, the rate of momentum change in the electron rest frame is not zero, contrary to the case of Thomson limit or synchrotron emission. One must take it into account in computing the energy loss rate in the blob rest frame which is not a Lorentz invariant anymore (Blumenthal & Gould 1970). In the head-on approximation the integral (11) and (12) over ε_1^* and Ω_1^* can be readily performed leading to:

$$\frac{dp'_x}{dt'} = -\sigma_T \int dn^* (f_p(\varepsilon^*) + \beta' f_E(\varepsilon^*)). \quad (14)$$

The two functions f_p and f_E are given by:

$$f_p(\varepsilon^*) = (1 + \varepsilon^*) f(\varepsilon^*), \\ f_E(\varepsilon^*) = -\varepsilon^* f(\varepsilon^*),$$

where the function $f(\varepsilon^*)$ corresponds to the ultrarelativistic case ($\beta' = 1$) and is given by:

$$f(\varepsilon^*) = \frac{1}{8} \frac{18\varepsilon^* + 102\varepsilon^{*2} + 186\varepsilon^{*3} + 102\varepsilon^{*4} - 20\varepsilon^{*5}}{\varepsilon^{*3} (1 + 2\varepsilon^*)^3} \\ + \ln(1 + 2\varepsilon^*) \times \\ \frac{1}{8} \frac{(-9 - 141\varepsilon^{*2} - 60\varepsilon^* - 126\varepsilon^{*3} - 12\varepsilon^{*4} + 24\varepsilon^{*5})}{\varepsilon^{*3} (1 + 2\varepsilon^*)^3}.$$

We then use these expressions in equation (8).

We can estimate the errors in the two extreme regimes described above. In the head-on approximation the first corrections are roughly $\frac{1}{\gamma^2}$, while in the Thomson limit these corrections are $\sim \gamma \langle \varepsilon \rangle$. Here $\langle \varepsilon \rangle \propto \dot{M}^{1/4} M^{-1/2}$ is the average photon energy emitted from accretion disc. We connect the two regimes by defining a critical Lorentz factor γ'_{crit} for which errors in the head-on approximation ($\gamma' > \gamma'_{crit}$) and in the Thomson limit ($\gamma' < \gamma'_{crit}$) are of same order. This gives $\gamma'_{crit} \sim \langle \varepsilon \rangle^{-1/3}$. So we may have errors of order of $\frac{1}{\gamma'_{crit}^2} \sim \gamma'_{crit} \langle \varepsilon \rangle \sim \langle \varepsilon \rangle^{2/3}$. For AGN $\langle \varepsilon \rangle \sim 10^{-4}$ and we find $\gamma'_{crit} \sim 20 - 30$ with a maximum error $\sim 0.2\%$ while for a microquasar $\langle \varepsilon \rangle \sim 10^{-2}$ and $\gamma'_{crit} \sim 5$ with a maximum error $\sim 5\%$.

2.4 Equation of motion

Following Phinney (1982) we determine the acceleration of pair plasma by considering the conservation of stress-energy

tensor leading to Phinney's (7) and (8) equations in the bulk rest frame:

$$\frac{\partial}{\partial t'} [(\rho' + p')\gamma_b - p/\gamma_b] = F'^0 + \beta_b F'^z, \quad (15)$$

$$\frac{\partial}{\partial t'} [(\rho' + p')\gamma_b \beta_b] = F'^z + \beta_b F'^0. \quad (16)$$

Combining these two equations and for a reheated relativistic plasma (with $p' = \rho'/3$) one finds the equation of motion (with $dz' = \beta_b dt'$ and $z = z'$):

$$\frac{d\gamma_b}{dz} = \frac{F'^z}{\rho'} \frac{1}{\frac{1}{3\gamma_b^2} + 1}. \quad (17)$$

To compute the radiative force by equation (14) we need the differential photon distribution in each electron rest frame.

For this we use the Lorentz invariant $\frac{dn}{\epsilon}$ (see Blumenthal & Gould 1970) and the relation between energy in the accretion disc frame and the electron rest frame:

$$\epsilon^* = \gamma_b(1 - \beta_b \mu_s)\gamma(1 - \beta \mu')\epsilon. \quad (18)$$

In the last equation μ_s is the cosinus of the angle between photon direction and jet axis in the accretion disc frame (see figure 1) and $\mu' = \mu'_e \mu'_s + (1 - \mu'_e)^{1/2}(1 - \mu'_s)^{1/2} \cos \phi'_e$ is the cosinus between the electron and photon direction in the bulk rest frame. We use the averaged scattered photon energy over the azimuthal angle ϕ_e , and take equation (18) with $\mu' = \mu'_e \mu'_s$. Finally we integrate equation (17) between $z = 10 r_g$ and $z = 10^4 r_g$ (galactic case) or $z = 10^5 r_g$ (extragalactic case) for different configurations to determine the final bulk Lorentz factor.

3 RESULTS

3.1 Equilibrium Lorentz factor

In any axisymmetric radiation field different from a plane wave, there exists an equilibrium Lorentz factor γ_{beq} for which the radiation force vanishes ($F'^z(\gamma_{beq}) = 0$, see figure 3). For $\gamma_b > \gamma_{beq}$ the pair plasma sees much more photons coming forward and then decelerates, while if $\gamma_b < \gamma_{beq}$ the plasma is pushed by radiation. The qualitative behaviour of a general solution of equation (17) is thus the following: γ_b is first set to the value γ_{beq} . This value increases gradually until an altitude $z = z_{crit}$ radiation force becomes too weak to accelerate the plasma. So it follows a ballistic motion at a constant Lorentz factor $\gamma_{b\infty}$. This mechanism ensures that in most cases the initial value of γ_b does not influence the terminal value, if the blob is injected below z_{crit} .

The Thomson regime has been well studied by various authors (Phinney 1982, 1987, Marcowith et al. 1995, Sikora et al. 1996). In this case the equilibrium Lorentz factor is determined by the simple condition $H' = 0$, that is the radiation flux vanishes in the blob rest frame. Analytical calculations in the Thomson regime give the behaviour of the equilibrium Lorentz factor and the solutions of the equation of motion for a standard accretion disc (Shakura & Sunyaev 1973). This yields $\gamma_{beq} \propto z^{1/4}$ for $z < r_e$ and $\gamma_{beq} \propto z$ for $z > r_e$ (see Appendix A for this case). Figure 3 shows the function γ_{beq} obtained in the Thomson limit for different values of r_e in comparison with these two asymptotic regimes. Note that for decreasing size of the accretion

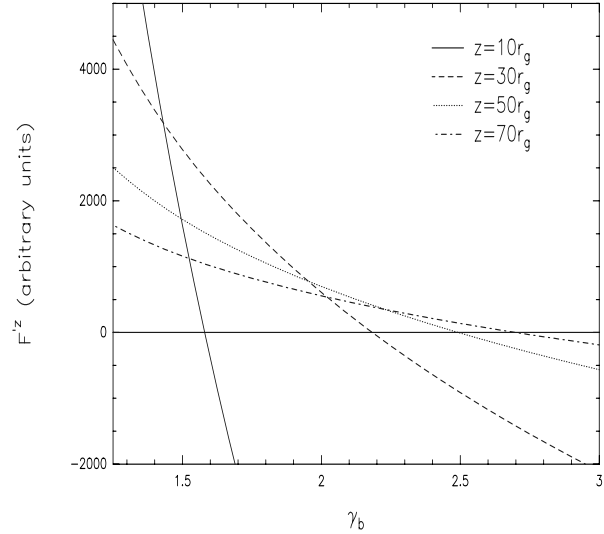


Figure 2. The radiative force as a function of the bulk Lorentz factor γ_b at different altitudes from the central black hole.

disc, the radiation field is more and more anisotropic and the function γ_{beq} increases more rapidly with z . For $z_{crit} < r_e$ one finally gets for a hot plasma $\gamma_{b\infty} \propto \left(\frac{\langle \gamma'^2 \rangle l}{\langle \gamma' \rangle}\right)^{1/7}$, while for $z_{crit} > r_e$, $\gamma_{b\infty} \propto \left(\left(\frac{r_i}{r_e}\right)^{3/4} \frac{\langle \gamma'^2 \rangle l}{\langle \gamma' \rangle}\right)^{1/4}$ (see Appendix A). $l = \frac{\sigma_T L}{4\pi m_e c^3 r_i}$ is the compactness of the source, and $\langle f \rangle = \left(\int n'_e(\gamma') d\gamma'\right)^{-1} \times \int f n'_e(\gamma') d\gamma'$.

Figure 4 shows the equilibrium Lorentz factor calculated including KN corrections for different configurations. We compare the results with the correspondant Thomson solution. The effect of the KN corrections is to reduce the contribution of high energetic collisions ($\epsilon^* \geq 1$) in the net radiation force seen by the plasma. Since the more energetic photons come from the inner part of the accretion disc, in the blob rest frame they contribute to accelerate the plasma. On the other hand the outer and colder part contribute to decelerate it. We then expect that the equilibrium Lorentz factor is reduced when including KN corrections as shown in figure 4. The importance of the difference depends on the particle and photon distributions. It is predominant for microquasars in which accretion disc radiates more energetic photons than in the extragalactic case.

3.2 Influence of the different parameters

3.2.1 General considerations

To determine the terminal Lorentz factor for different configurations, we solve numerically the equation of motion for various radiation fields and particle distributions. We show in figure 5 typical solutions in the case of a stellar black hole. The terminal value of the bulk Lorentz factor does not depend on the initial value of γ_b init as discussed in paragraph 3.1. The general behaviour of the solution discussed

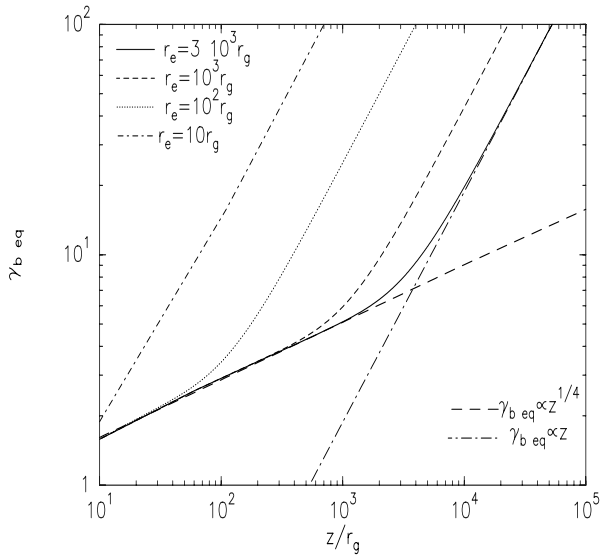


Figure 3. Equilibrium Lorentz factor $\gamma_{b\text{eq}}$ as a function of z in the Thomson limit. $\gamma_{b\text{eq}}$ is given for $r_e = 10 r_g$, $r_e = 10^2 r_g$, $r_e = 10^3 r_g$ and $r_e = 3 \cdot 10^3 r_g$. We also represent the two asymptotic regimes $\gamma_{b\text{eq}} \propto z^{1/4}$ for $z < r_e$ and $\gamma_{b\text{eq}} \propto z$ for $z > r_e$, with $r_e = 3 \cdot 10^3 r_g$.

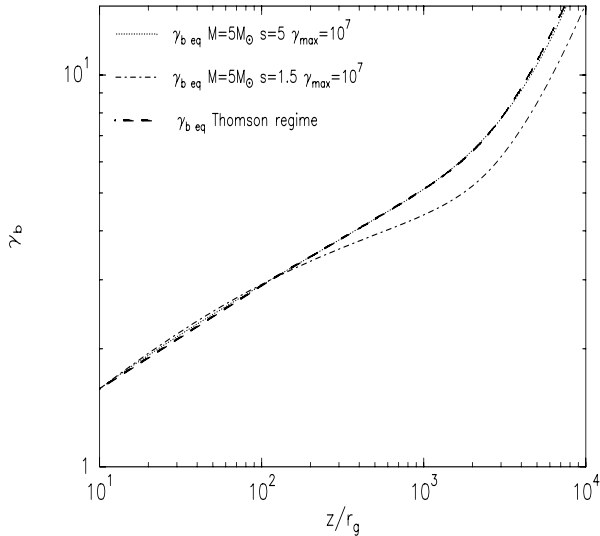


Figure 4. The Equilibrium Lorentz factor calculated including KN corrections compared to Thomson solution. The figure corresponds to a stellar black hole $M = 5M_\odot$ with $\gamma_{\max} = 10^7$ for spectral index $s = 1.5$ and $s = 5$. The external radius is $r_e = 3 \cdot 10^3 r_g$ and $L = L_{Edd}$.

in this paragraph still holds even including KN corrections. The critical point z_{crit} is reached rather close to the central engine (before 10^4 Schwarzschild radii). For $z > z_{crit}$ the motion is nearly ballistic and so independent of the radiation force which has become too weak. It is so independent of any variation of the pair distribution unless these variations strengthen the radiation force. This scenario would require a more efficient acceleration mechanism when moving away

from the central source, which is very unlikely. Therefore our assumption of a stationary pair energy distribution on a large range of z does not influence strongly the terminal value of γ_b , or in other words this value is essentially determined by the local parameters at the critical distance.

3.2.2 Influence of the energy upper cut-off and spectral index

Figure 6 illustrates the influence of the spectral index (for $1.5 \leq s \leq 5$) and the energy cut-off (for $10^3 \leq \gamma_{\max} \leq 10^7$) on the terminal Lorentz factor. We chose $M = 5M_\odot$ representative for stellar black holes and $M = 10^9 M_\odot$ for supermassive black holes. The calculations were carried out for $L = L_{Edd}$ and $L = 0.1L_{Edd}$, where L is the luminosity of the accretion disc.

Results are very sensitive to the spectral index value. There are 3 different behaviours according to the value of s .

(i) for $s < 2$ there exists a maximum terminal Lorentz factor as a function of γ_{\max} and the curve intercepts the other ones.

(ii) for $2 < s < 3$ there still exists a maximum, but less pronounced. The variation as a function of γ_{\max} are smoother.

(iii) for $s > 3$ no variation with γ_{\max} .

We find that for low value of γ_{\max} , our solutions agree with the Thomson regime solutions. Nevertheless KN corrections reduce the efficiency of the Compton rocket effect. As a matter of fact, in the Thomson regime, an increase of γ_{\max} leads to an increase of $\langle \gamma^2 \rangle$ (for $s < 3$) and so of $\gamma_b\infty$. This mechanism is valid until KN corrections begin to dominate, roughly when $\gamma_{\max}\langle \varepsilon \rangle \sim 1$. So when γ_{\max} is greater than $\langle \varepsilon \rangle^{-1}$ the radiation force does not increase anymore whereas the plasma inertia ρ' is much more important. This leads to a less efficient acceleration mechanism. This effect is larger for small indexes explaining the inversion of the curve for high γ_{\max} . Indeed we find that acceleration is much more efficient for $s = 2$ and $\gamma_{\max} = 10^7$ than for $s = 1.5$ and the same value of γ_{\max} , in the case of stellar black hole. When steepening the pair distribution, the radiation force is dominated by the low energy part of the distribution. This fact explains why no variation is apparent with γ_{\max} for $s > 3$. The plasma behaves dynamically as a cold one, and we find small value of terminal Lorentz factor. Finally including KN corrections in the calculations gives rise to an absolute upper limit to maximal Lorentz factor for a given luminosity.

3.2.3 Influence of the black hole mass

As discussed above the influence of the mass of the central black hole is predominant. Stellar black holes with soft X-ray emission ($\langle \varepsilon \rangle \sim 10^{-2}$) are less efficient in accelerating blob of pair plasma than supermassive black hole with softer radiated emission ($\langle \varepsilon \rangle \sim 10^{-4}$), because KN saturation effects occur at much lower energy. A more realistic description of the accretion disc around stellar black holes reinforces this discrepancy. As shown in figure 7 the radiation emitted from a two-temperature disc (Shapiro et al. 1976) leads to smaller $\gamma_b\infty$ than in the case of standard accretion disc radiation. Because it is well established that accretion disc around stellar black holes should radiate up to a few keV (as in a two-temperatures disc), KN corrections play an important role in this case.

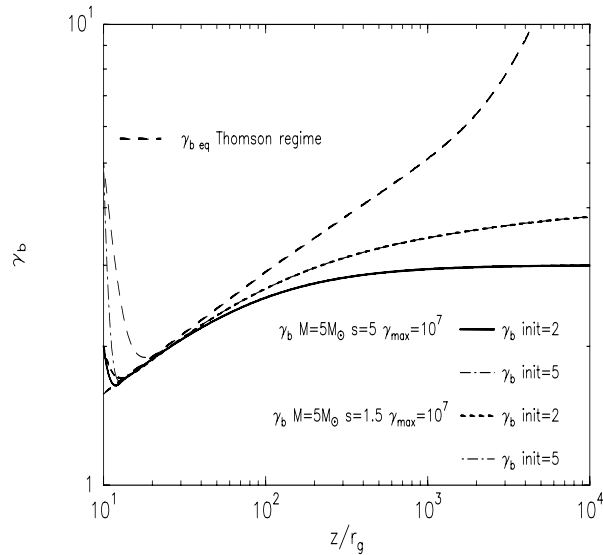


Figure 5. Solutions of the equation of motion in the case of a stellar black hole ($M = 5M_{\odot}$). We chose two different initial conditions $\gamma_b \text{ init} = 2$ and $\gamma_b \text{ init} = 5$. $r_e = 310^3 r_g$ and $L = L_{Edd}$.

3.2.4 Influence of the luminosity

As $\langle \varepsilon \rangle \propto \dot{M}^{1/4} M^{-1/2}$, the luminosity of the disc also directly influences the maximum of the function $\gamma_{b\infty}$ as a function of γ_{max} . As shown in figure 6, the maximum takes place at higher γ_{max} when the luminosity decreases. Besides less luminous systems contribute to a lower radiation force and so to a less efficient acceleration. In the Thomson regime one has a dependance $\gamma_{b\infty} \propto L^{1/7}$.

3.2.5 Effect of scattered radiation

All the results described above are obtained when studying the disc radiation alone. We also include in our calculation BLR radiation fields corresponding to two cases:

- a) re-emission from a ring located between r_1 and r_2 and with an emissivity given by equation (5)
- b) re-emission from spherically distributed matter at a distance r_0 from the central black hole with an emissivity given by equation (6).

Figure 8 displays the equilibrium Lorentz factor in the presence of a BLR located between $r_1 = 10^4 r_g$ and $r_2 = 10^5 r_g$ (case a), figure 8) in the Thomson regime. We also plotted the equilibrium Lorentz factor including KN corrections as well as the solution of the equation of motion for a plasma with $s = 2$ and $\gamma_{max} = 10^5$. As one can see, the effect of BLR on $\gamma_{b\infty}$ is very weakened by KN corrections. This can be understood because the photons coming from the BLR are blueshifted by the relativistic motion in the blob rest frame whereas the photons coming from the disc are redshifted. So the dragging force from the BLR is much more reduced by KN corrections than the accelerating one due to disc photons. Due to the weakness of the radiation field, the dynamical solution $\gamma_b(z)$ is still less affected than the

equilibrium value. The case of a spherical shell located at $r_0 = 10^4 r_g$ (case b)) is illustrated in figure 9. One can see that the diffused radiation field strongly affects the motion that is almost stopped at the crossing of the shell, where radiation density is dominated by the isotropically scattered photons. However, the plasma is quickly reaccelerated after the crossing, and high Lorentz factor can be reached again.

Sikora et al. (1996) argued that scattered radiation should lead to efficient radiation drag. However, the influence of scattered radiation is strongly governed by the position of scattering clouds with respect to the critical distance z_{crit} : if they lie below this critical distance, the plasma will be temporarily braked during the crossing of scattering region, but will be quickly reaccelerated after it. If the clouds lie above z_{crit} , the terminal Lorentz factor can indeed be strongly affected. Figure 10 and 11 display the terminal Lorentz factor as a function of γ_{max} for different distances of the BLR. It can be seen that if it is close enough, the BLR can give still higher Lorentz factor than for the disc alone for the highest value of γ_{max} . This is because the solid angle subtended by it at z_{crit} is so small that its radiation field has an accelerating rather than decelerating effect. But even for a BLR between 10^4 and $10^5 r_g$, terminal Lorentz factor around 10 are clearly reachable. We conclude that the presence of broad lines can affect $\gamma_{b\infty}$, but does not prevent in general highly relativistic motions.

We also discuss the effect of a possible emission from a hot dusty torus surrounding the central black hole outside the BLR region. The effect of such a scattered radiation field is much more important because KN corrections are here almost negligible. Figure 12 shows the terminal Lorentz factor in the presence of an IR emitting ring heated at $T = 1500K$, located between r_3 and r_4 . It is obvious that the terminal Lorentz factor is strongly reduced to values around 3 for the less favourable case ($r_3 = 10^4 r_g$, $r_4 = 10^5 r_g$). The situation is a little less dramatic for more distant sources ($r_3 = 10^5 r_g$, $r_4 = 10^6 r_g$) because the isotropic radiation density is lowered, and $\gamma_{b\infty}$ of 5 can be reached.

3.2.6 Influence of the accretion disc size

For small value of r_e the radiation is more anisotropic and so more efficient to accelerate the pair plasma (see figure 13). In this figure $r_e = 10 r_g$ and we show the solutions for which we obtain the largest $\gamma_{b\infty}$ in extragalactic and galactic cases. In this configuration the radiation force is more efficient and $\gamma_{b\infty}$ can be as high as 60 in the extragalactic case. The dependance on s and γ_{max} is shown in figure 14, where we extend the previous calculation to the case $r_e = 10 r_g$. We find the same global behaviour of $\gamma_{b\infty}$ with spectral index and γ_{max} .

4 COMPARISONS WITH OBSERVATIONS

Our model gives good agreement with observations of relativistic blob ejection in AGN and microquasars for the 'disc alone' solution. Figure 6 shows that in the most favourable configuration ($s = 1.5$, $\gamma_{max} \sim 10^6$ and $L = L_{Edd}$) Compton rocket effect is able to accelerate pair plasma up to Lorentz factor $\gamma_{b\infty} \geq 20$. This value is only gradually reached, the jet being much slower at small distances. One can obtain higher

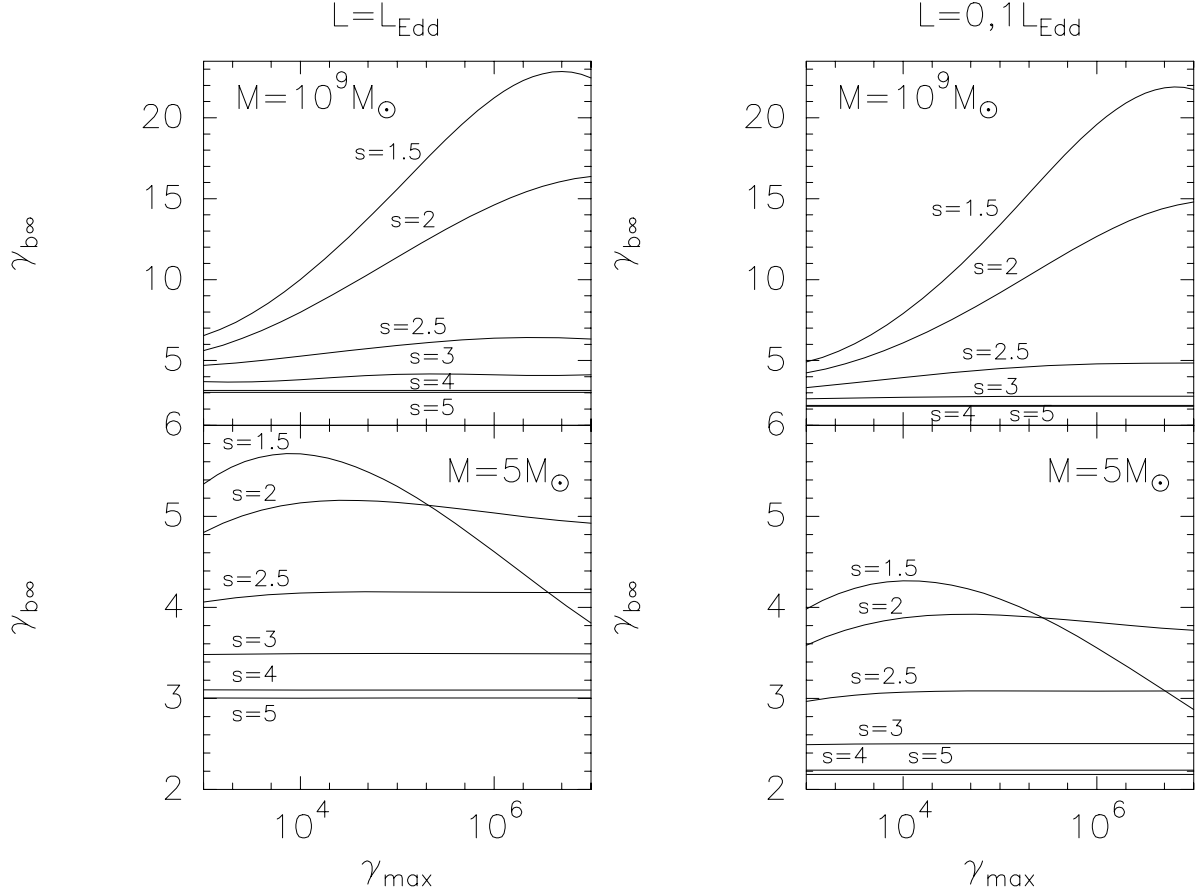


Figure 6. Terminal Lorentz factor $\gamma_{b\infty}$ as a function of γ_{max} for different value of spectral index s . The two top pannels correspond to $M = 10^9 M_\odot$ black hole with $r_e = 3.10^3 r_g$, $L = L_{Edd}$ (left) and $L = 0.1 L_{Edd}$ (right). The two bottom pannels correspond to $M = 5 M_\odot$ black hole with $r_e = 3.10^3 r_g$, $L = L_{Edd}$ (left) and $L = 0.1 L_{Edd}$ (right).

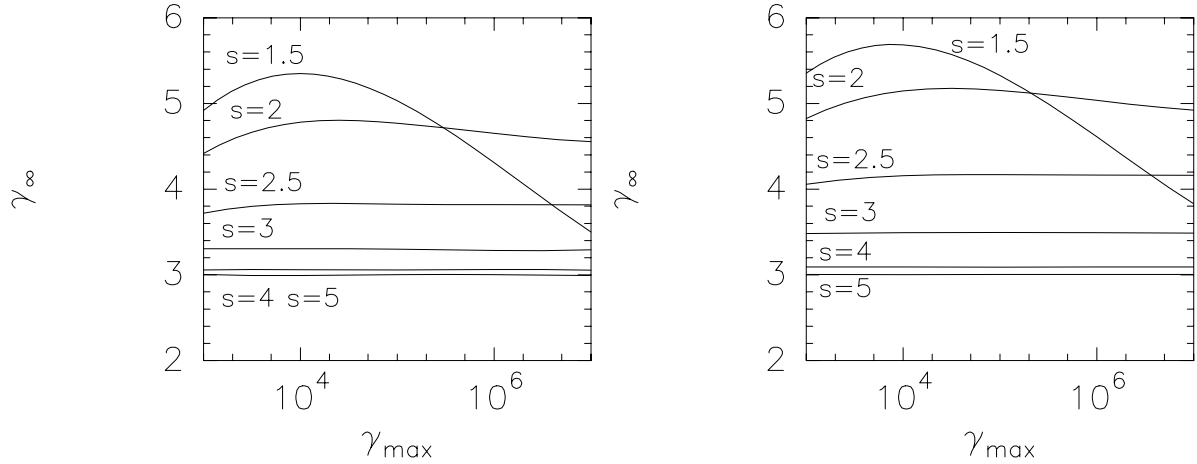


Figure 7. Comparisons of terminal Lorentz factor for a standard accretion disc (right) and a two-temperature disc (Shapiro et al. 1976) extended up to $15 r_g$ (left). In both case $r_e = 310^3 r_g$, $M = 5 M_\odot$ and the accretion rate is the Eddington one.

value for super-Eddington systems. One can notice that observations of the faster extragalactic superluminal motion correspond to such value of bulk Lorentz factor (Vermeulen

& Cohen 1994).

This value is however strongly dependent on the spectral index s and the high energy particle distribution cut-off

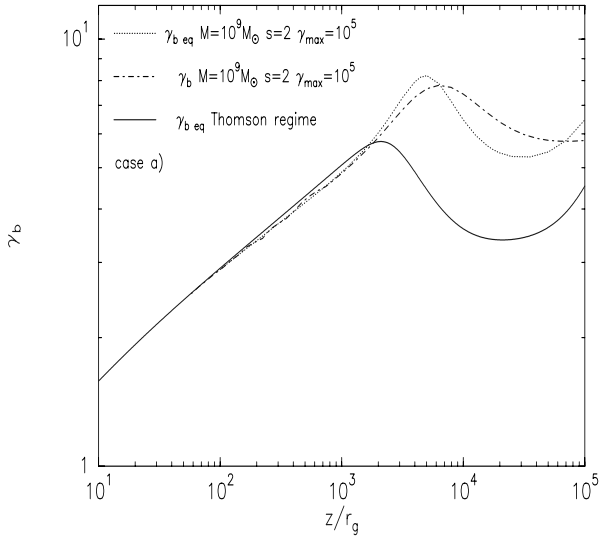


Figure 8. Equilibrium Lorentz factor as a function of z for radiation coming from an accretion disc and BLR radiation from a ring located between $r_1 = 10^4 r_g$ and $r_2 = 10^5 r_g$. The emissivity is described by equation (5) with $\chi = 0.1$ and $\alpha = 2$. We also show the solution of the equation of motion for this case. The solid curve shows $\gamma_{b\text{eq}}$ in Thomson regime. The plasma parameters are $s = 2$ and $\gamma_{\text{max}} = 10^5$. The black hole mass is $M = 10^9 M_\odot$ and $L = L_{\text{Edd}}$.

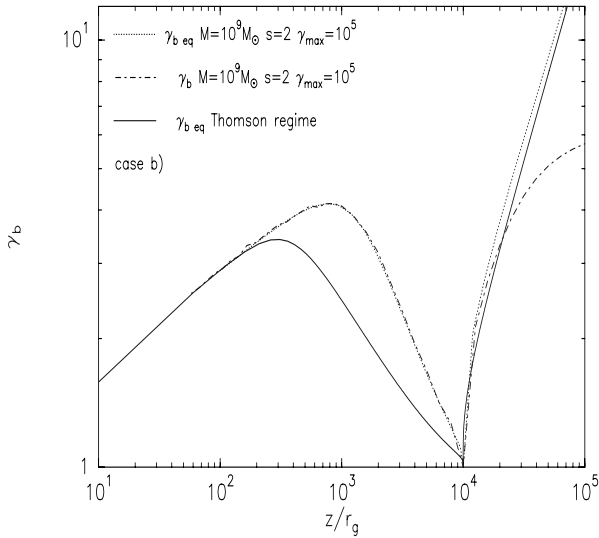


Figure 9. Same as figure 8 for a BLR radiation from a shell located at $r_0 = 10^4 r_g$. The emissivity is described by equation (6) with $\chi = 0.1$.

γ_{max} . The precise value of s is not obvious to derive from observations. High energy spectra show typical X-ray spectral indexes around 0.5, which correspond to $s \simeq 2$. There is very often a spectral break in the MeV range: this could be attributed to a break in the particle distribution, that would correspond to $\gamma_{\text{max}} = 10^2$. However, Marcowith et al. (1995) have shown that this break could be very well reproduced

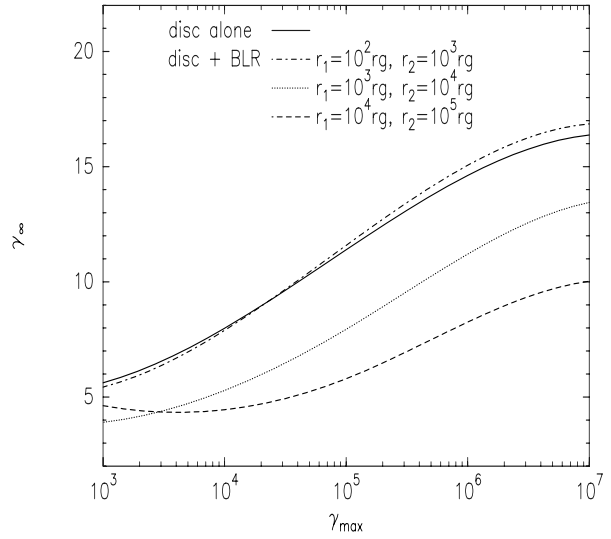


Figure 10. Terminal Lorentz factor $\gamma_{b\infty}$ as a function of γ_{max} for the spectral index $s = 2$. The solid line shows the solution obtained including KN corrections for a standard accretion disc. The scattered radiation is described by equation (5) with $\chi = 0.1$, $\alpha = 2$ and different locations of the BLR ring.

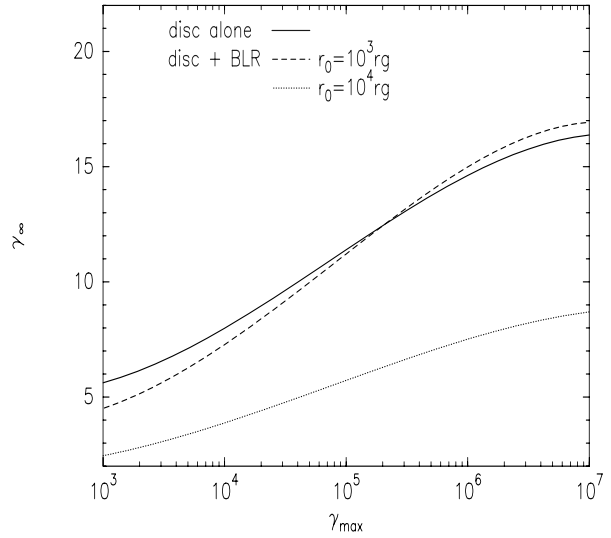


Figure 11. Same as figure 10 for scattered radiation described by equation (6) with $\chi = 0.1$ and different locations of the BLR shell.

by $\gamma - \gamma$ absorption with an actual particle distribution giving the primary photon spectrum that can extend to much higher energy. So high energy spectra may not be good indicators of the upper cut-off γ_{max} . Moreover, the high energy emission probably takes place at relatively small distances (around $10^2 r_g$) from the center, well below z_{crit} : the final bulk Lorentz factor is not yet reached at this distance. On the other hand, the detection of photons with at least 30 GeV, and even above TeV for some BL Lacs, implies an upper cut-off $\gamma_{\text{max}} \geq 10^5$.

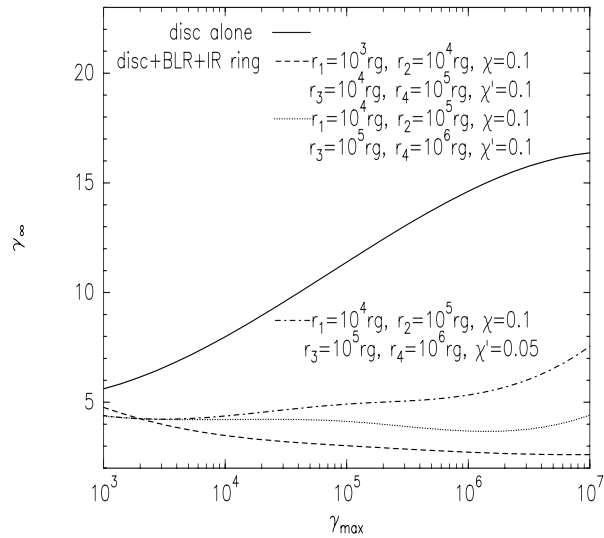


Figure 12. The influence of a dusty ring combined with a BLR on the terminal Lorentz factor $\gamma_{b\infty}$ as a function of γ_{max} , for the spectral index $s = 2$. The solid line shows the solution obtained including KN corrections for a standard accretion disc. The BLR ring emissivity is described by equation (5) with $\chi = 0.1$, $\alpha = 2$. The dusty ring emissivity is given by equation (7) with $\chi' = 0.1$ or $\chi' = 0.05$. We chose different locations for these two components.

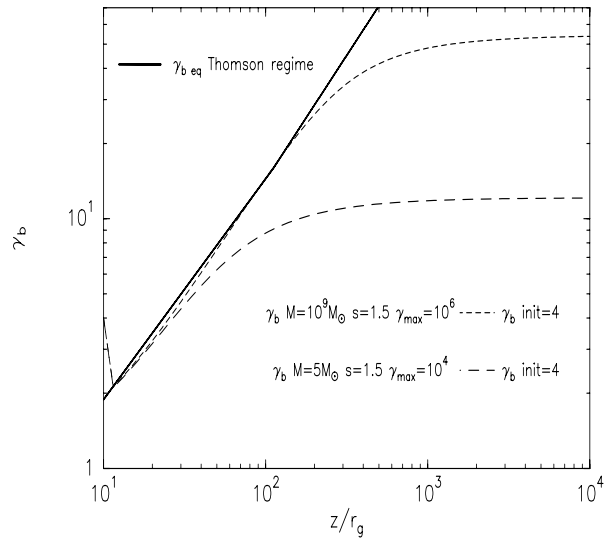


Figure 13. Solutions of the equation of motion for a supermassive black hole ($M = 10^9 M_\odot$) and a stellar black hole ($M = 5 M_\odot$) with a compact accretion disc. $r_e = 10 r_g$ and $L = L_{Edd}$. γ_b init is the initial condition of the solution. We also represent the equilibrium Lorentz factor in Thomson regime.

Radio spectral indexes are also difficult to assess because of synchrotron self-absorption, especially for radio-flat quasars where the observed spectrum results probably from the superposition of many self-absorbed spectra. The optically thin index ranges mostly from 0.5 to 1, which corresponds to $2 \leq s \leq 3$. With reasonable parameters

($2 \leq s \leq 3$ and $\gamma_{max} \leq 10^5$), our model predicts typical values $4 \leq \gamma_{b\infty} \leq 10$ which are the most frequently observed (Vermeulen & Cohen 1994). Moreover, as shown in Sect. 3.2.5, KN effects prevent from strong Compton drag induced by BLR radiation in the vicinity of the central black hole. The fastest superluminal motions may be attributed to those objects for which the BLR is weak and/or closest to the central object.

On the other hand, the slowest motions ($\gamma_{b\infty} \leq 4$) can be obtained in the presence of a rich and extended environment of scattering material, such as BLR clouds and dusty torus. The presence of dust is inferred from an enhancement in the near infrared in some quasars spectra (Baird 1987). Nevertheless a nonthermal infrared component, attributed to synchrotron radiation from the relativistic jet, is also usually observed in radio-loud AGN. This component is generally predominant in flat spectrum radio quasars (Neugebauer et al. 1986) and is necessary to explain rapid variations observed in infrared flaring objects. We can speculate that these objects with the largest superluminal motion are those where the scattered thermal component is particularly weak. Such 'nonthermal' objects should not suffer strong radiation drag, while 'thermal' ones should have the lowest terminal Lorentz factors. In conclusion the diversity among observed superluminal motions can be reproduced by our model by considering both influence of the plasma acceleration mechanism and AGN environment.

The observed value of Lorentz factor of about 2.5 for the two microquasars (GRS1915+105, Mirabel & Rodriguez 1994 and GROJ1655-40, Hjellming & Rupen 1995) with large spectral indexes (respectively $s \sim 4$, Finoguenov et al. 1994 and $s \sim 4.6$, Harmon et al. 1995) are consistent with our results. We show figure 15 the dependence of $\gamma_{b\infty}$ on compactness of the source for $s = 4$ and $s = 5$. We find that observations require $L \sim 0.2 - 0.3 L_{Edd}$, which is very close to the result by Li & Liang (1996). This result is not strongly affected by the mass of the central black hole if the compactness of the source remains the same. The steep spectra observed in these two objects ensure us that the terminal Lorentz factor is just dependant on the low energy cut-off of the electron distribution. In this case a more realistic description of the accretion disc emission does not change our results for such spectral indexes (figure 7). Yet the maximal value of $\gamma_{b\infty}$ is model dependant. The part of high energy emission contributes to decrease this value from the one obtained for a standard accretion disc. We find that value of about 6 can be reached in the most favourable case.

Finally, $\gamma_{b\infty}$ is much higher for a small sized accretion disc. We find value of about 60 in the case of an external radius of $10 r_g$ in the case of supermassive black hole.

5 CONCLUSION

We have considered the bulk acceleration of an electron-positron pair plasma in the vicinity of a central black hole. The acceleration is due to Compton rocket effect on the plasma and the radiation force originates from a standard accretion disc emission. The pair plasma is continuously reheated by an efficient turbulent mechanism which takes place in the frame of the 'two-flow' model. Thus we assumed in our calculations a stationary power-law energy distribution for the pair. We included KN corrections in the computation

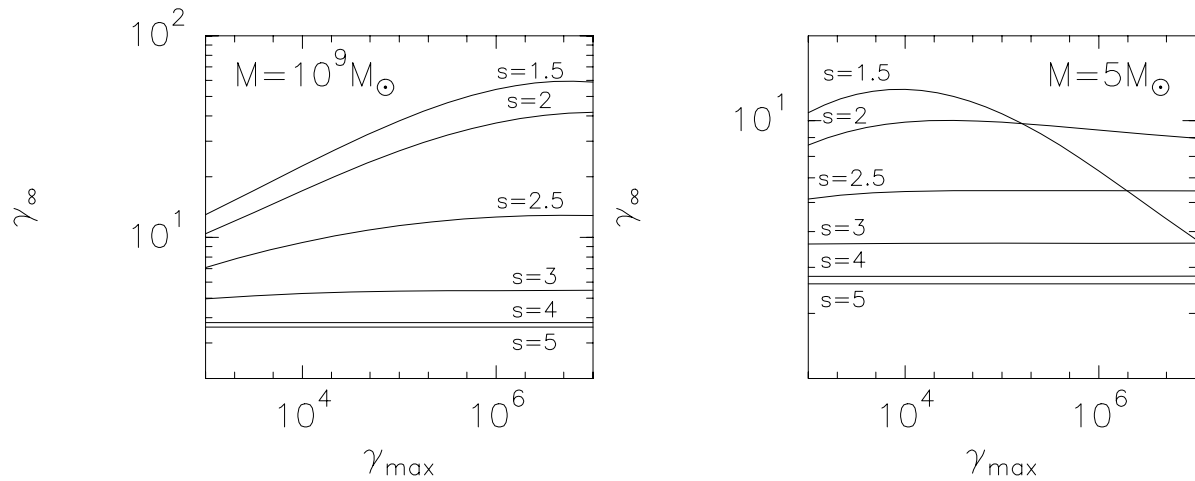


Figure 14. Terminal Lorentz factor $\gamma_{b\infty}$ as a function of γ_{max} for different value of spectral index s . The two pannels correspond to $r_e = 10 r_g$, $L = L_{Edd}$, $M = 10^9 M_\odot$ (left) and $M = 5 M_\odot$ (right).

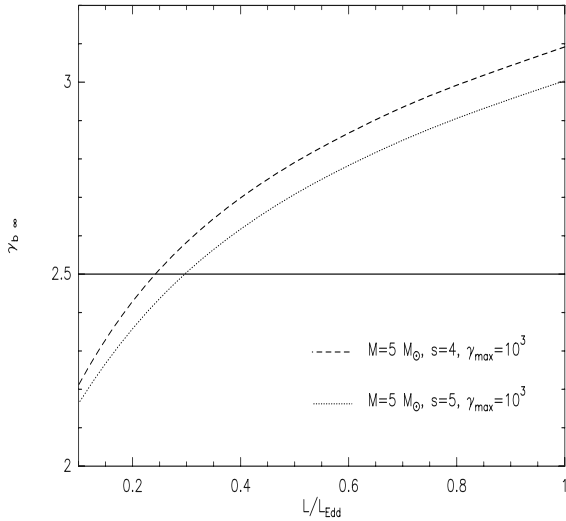


Figure 15. The terminal Lorentz factor as a function of L/L_{Edd} and for two spectral indexes ($s = 4$ and $s = 5$). $M = 5 M_\odot$, $\gamma_{max} = 10^3$.

of the radiation force, and solved numerically the equation of motion. We studied configurations relevant to relativistic motion in AGN and galactic microquasars. The main results of our calculations can be summarized as follows:

(i) For a given luminosity, the terminal Lorentz factor $\gamma_{b\infty}$ admits an absolute maximum due to KN corrections. Values of about 20 can be reached in the extragalactic case, for sufficiently flat spectrum ($s \sim 1.5$) and accretion at the Eddington rate which may correspond to the highest observed relativistic motion. For more reasonable plasma parameters ($s \leq 2$ and $\gamma_{max} \leq 10^6$) the Compton rocket effect can account for the typical value of terminal Lorentz factor inferred from observations ($\gamma_{b\infty}$).

(ii) Scattered radiation from extended BLR or dusty torus can brake efficiently relativistic motion, even for a high energy plasma. This Compton drag and a weak plasma heating can be responsible for the lowest terminal Lorentz factor observed. The highest superluminal motion could be attributed to objects with particularly weak diffuse component and very efficient heating.

(iii) For stellar black holes KN corrections are important leading to smaller values than for a supermassive black hole. Recent observations of relativistic ejection in galactic microquasars are consistent with our results.

ACKNOWLEDGMENTS

We would like to thank the anonymous referee for his helpful remarks, especially for the description of scattered radiation.

REFERENCES

- Barvainis, R. , 1987, ApJ, 320, 537
- Blumenthal, G. R., Gould, R. J., 1970, Rev. of mod. physics, 42, 2237, Bremsstrahlung, Synchrotron radiation, and Compton scattering of high-energy electrons traversing dilute gases
- Finoguenov, A. et al., 1994, ApJ, 424, 940
- Harmon, B. A. et al., 1995, Nature, 374, 703
- Henri, G., Pelletier, G., 1991, ApJ Letters, 383, L7
- Henri, G., Pelletier, G., Roland, J., 1993, ApJ Letters, 404, L41
- Hjellming, R. M., Rupen, M. P., 1995, Nature, 375, 464
- Li, H., Liang, E. P., 1996, ApJ, 458, 514
- Marcowith, A., Henri, G., Pelletier, G., 1995, MNRAS, 277, 681
- Mirabel, I. F., Rodriguez, L. F., 1994, Nature, 371, 46
- Neugebauer, G. et al., 1986, ApJ, 308, 815
- O'Dell, S. L., 1981, ApJ Letters, 243, L147
- Phinney, E. S., 1982, MNRAS, 198, 1109
- Phinney, E. S., 1987, in Superluminal Radio Sources, ed. Zensus, J. A. & Pearson, T. J., 301 (Cambridge, UK)
- Rybicki, G. B., Lightman, A. P., 1979, Radiative Processes in Astrophysics (New York: John Wiley)
- Shakura, N. I., Sunyaev, R. A. , 1973, A&A, 24, 337
- Shapiro, S. L., Lightman, A. L., Eardley, D. M., 1976, ApJ, 204, 187

Sikora, M., Sol, H., Begelman M. C., Madejski, G. M., 1996, MNRAS, 280, 781
 Sol, H., Pelletier, G., Asséo, E., 1989, MNRAS, 327, 411
 Sunyaev, R. A., Titarchuk, L. G., 1980, A&A, 86, 121
 Tingay, S. J. et al., 1995, Nature, 374, 141
 Vermeulen, R. C., Cohen, M. H., 1994, ApJ, 430, 467

APPENDIX A: EQUILIBRIUM LORENTZ FACTOR AND TERMINAL LORENTZ FACTOR IN THOMSON REGIME

Eddington parameters are defined as follows:

$$\begin{aligned} J &= \frac{1}{4\pi} \int I_\nu(\Omega) d\Omega d\nu, \\ H &= \frac{1}{4\pi} \int \mu I_\nu(\Omega) d\Omega d\nu, \\ K &= \frac{1}{4\pi} \int \mu^2 I_\nu(\Omega) d\Omega d\nu. \end{aligned} \quad (\text{A1})$$

Marcowith et al. (1995) show that these parameters can be expressed in the case of standard accretion disc (Shakura & Sunyaev 1973) as a function of the integral:

$$I(\alpha, \beta, \gamma) = \int_1^{u_e} [1/u^\alpha (1 + \varepsilon^2 u^2)^\beta] [1 - (1/u)^{1/2}]^\gamma du, \quad (\text{A2})$$

with $u = r/r_i$, $u_e = r_e/r_i$ and $\varepsilon = r_i/z$. They obtain:

$$\begin{aligned} J &= (L/8\pi^2 r_i^2) (1 - 2b/3)^{-1} \varepsilon^2 I(2, 3/2, 1), \\ H &= (L/8\pi^2 r_i^2) (1 - 2b/3)^{-1} \varepsilon^2 I(2, 2, 1), \\ K &= (L/8\pi^2 r_i^2) (1 - 2b/3)^{-1} \varepsilon^2 I(2, 5/2, 1). \end{aligned} \quad (\text{A3})$$

They study the case $r_i < z < r_e$ for which $\varepsilon < 1$ and $u \geq 1$. They find that the equilibrium Lorentz factor is given by:

$$\gamma_{beq} \sim \varepsilon^{1/4} = \frac{z^{1/4}}{r_i^{1/4}} \quad (\text{A4})$$

In the case $z > r_e$ we have $\varepsilon u = r/z < 1$ for $1 < u < u_e$. So we can expand the term $(1 + \varepsilon^2 u^2)^{-\beta}$ into series:

$$(1 + \varepsilon^2 u^2)^{-\beta} = \sum_k (-1)^k \frac{\beta(\beta+1)\dots(\beta+k-1)}{k!} \varepsilon^{2k} u^{2k}. \quad (\text{A5})$$

Hence in the case $\alpha = 2$, $\gamma = 1$ and integrating over u , we obtain:

$$\begin{aligned} I(2, \beta, 1) &= \sum_k \varepsilon^{2k} (-1)^k \frac{\beta(\beta+1)\dots(\beta+k-1)}{k!} \\ &\times \left(\frac{u_e^{2k-1} - 1}{2k-1} - \frac{u_e^{2k-3/2} - 1}{2k-3/2} \right). \end{aligned} \quad (\text{A6})$$

The first coefficients in ε are then:

$$I(2, \beta, 1) = A_0 - \beta A_1 \varepsilon^2 + \frac{\beta(\beta+1)}{2} A_2 \varepsilon^4, \quad (\text{A7})$$

with

$$\begin{aligned} A_0 &= \frac{1}{3} - u_e^{-1} + \frac{2}{3} u_e^{-3/2} \sim \frac{1}{3}, \\ A_1 &= u_e - 2u_e^{1/2} + 1 \sim u_e, \\ A_2 &= \frac{u_e^3}{3} - \frac{2u_e^{5/2}}{5} + \frac{1}{15} \sim \frac{u_e^3}{3}. \end{aligned} \quad (\text{A8})$$

The equivalents are given for $u_e \gg 1$. This gives for the Eddington parameters:

$$\begin{aligned} J &= (L/8\pi^2 r_i^2) (1 - 2b/3)^{-1} \varepsilon^2 (A_0 - 3/2A_1 \varepsilon^2 + 15/8A_2 \varepsilon^4), \\ H &= (L/8\pi^2 r_i^2) (1 - 2b/3)^{-1} \varepsilon^2 (A_0 - 2A_1 \varepsilon^2 + 3A_2 \varepsilon^4), \\ K &= (L/8\pi^2 r_i^2) (1 - 2b/3)^{-1} \varepsilon^2 (A_0 - 5/2A_1 \varepsilon^2 + 35/8A_2 \varepsilon^4). \end{aligned} \quad (\text{A9})$$

The equilibrium Lorentz factor is $\gamma_{beq} = (1 - \beta_{beq}^2)^{-1/2}$ where

$$\beta_{beq} = x - (x^2 - 1)^{1/2}, \quad (\text{A10})$$

with

$$x = \frac{J + K}{2H}. \quad (\text{A11})$$

Using equations (A9) we find with $u_e \gg 1$:

$$x = 1 + \frac{1}{8} u_e^3 \varepsilon^4, \quad (\text{A12})$$

$$\beta_{beq} = 1 - \frac{u_e^{3/2}}{2} \varepsilon^2, \quad (\text{A13})$$

and finally

$$\gamma_{beq} = u_e^{-3/4} \varepsilon = \frac{z}{r_e^{3/4} r_i^{1/4}}. \quad (\text{A14})$$

The asymptotic solution of equation (17) is approximately $\gamma_{b\infty} = \gamma_{beq}(z_{crit})$, where z_{crit} is the location where the radiative force becomes to weak to maintain $\gamma_b(z) = \gamma_{beq}(z)$. This occurs when the evolution of γ_{beq} , i.e. $\Delta z_0 = \gamma_{beq}/(\text{d}\gamma_{beq}/\text{d}z) = \text{dlog}(z)/(\text{dlog}(\gamma_{beq}))$, is larger than the evolution of γ_b towards γ_{beq} , i.e. $\Delta z_1 = (\text{d}\gamma_b/\text{d}z)/(\gamma_b - \gamma_{beq})$. Using equation (17) one finds:

$$z_{crit} \sim \left(\frac{1}{\rho'} \frac{\text{d}F'^z}{\text{d}\gamma_b} \Big|_{\gamma_{beq}} \right)^{-1}. \quad (\text{A15})$$

In the Thomson regime we can use equation (9) and (10) which give in the relativistic case:

$$\frac{\text{d}F'^z}{\text{d}\gamma_b} = -\frac{\sigma_T}{c} \frac{8\pi}{3} \langle \gamma'^2 \rangle \frac{\text{d}H'}{\text{d}\gamma_b} = \frac{2H}{\gamma_b} (1 - x/\beta_b). \quad (\text{A16})$$

With (A9), (A12), (A13), (A14) and ignoring some terms of order unity one finally gets:

$$z_{crit} \sim \left(r_e^{9/4} r_i^{3/4} \frac{L\sigma_T}{m_e c^3} \frac{\langle \gamma'^2 \rangle}{\langle \gamma' \rangle} \right)^{1/4}, \quad (\text{A17})$$

and,

$$\gamma_{b\infty} \sim \left(l \left(\frac{r_i}{r_e} \right)^{3/4} \frac{\langle \gamma'^2 \rangle}{\langle \gamma' \rangle} \right)^{1/4}. \quad (\text{A18})$$

In the case $r_i < z < r_e$, using equation (A4) one finds:

$$z_{crit} \sim r_i \left(\frac{L\sigma_T}{m_e c^3 r_i} \frac{\langle \gamma'^2 \rangle}{\langle \gamma' \rangle} \right)^{4/7}, \quad (\text{A19})$$

and finally,

$$\gamma_{b\infty} \sim \left(l \frac{\langle \gamma'^2 \rangle}{\langle \gamma' \rangle} \right)^{1/7}. \quad (\text{A20})$$